Journal of Renewable Materials

Tech Science Press

DOI: 10.32604/jrm.2023.028046

ARTICLE

Investigation of the Thermal Decomposition Behavior of Oleuropein with Many Pharmacological Activities from Olive by Thermogravimetry

Jiaojiao Yuan[1], Su Tuo[1], Yangyang Liu[1], Jing He[1], Shao-Hwa Hu[1] and Junling Tu[2,*]

[1]School of Business and Trade, Dongguan Polytechnic, Dongguan, 523808, China

[2]School of Chemical Engineering and Energy Technology, Dongguan University of Technology, Dongguan, 523808, China

[*]Corresponding Author: Junling Tu. Email: tujl@dgut.edu.cn

Received: 28 November 2022 Accepted: 30 January 2023 Published: 26 June 2023

ABSTRACT

Due to the existence of poly-hydroxyl structures, the temperature may have an effect on the thermal stability of oleuropein for its applications. In the current study, the thermal decomposition process and kinetics behavior of oleuropein from the olive resource were researched by thermogravimetric theoretical analysis methods and non-isothermal kinetics simulation. The results of thermogravimetry analysis showed the whole thermal decomposition process of oleuropein involved two stages, with 21.22% of residue. It was also revealed that high heating rates of more than 20 K min^{-1} led to significant thermal hysteresis and inhibited the whole thermal decomposition behavior of oleuropein. Moreover, an investigation of the thermal decomposition kinetics indicated that the non-isothermal decomposition behavior followed a D3 model during the first stage (three-dimensional diffusion, Jander equation) and a D1 model in the second stage (one-dimensional diffusion). For the first and second thermal decomposition stages, the Kissinger, Friedman, Flynn-Wall-Ozawa, and Coats–Redfern four methods were applied to determine the activation energy (E = 143.72 and 247.01 kJ mol^{-1}) and Arrhenius preexponential factor (ln A = 26.34 and 42.45 min^{-1}), respectively. Therefore, the study will provide good theoretical guidance for thermal stability and thermal transformation application of oleuropein. It will be suitable for low-temperature applications in the cosmetic, food supplement and pharmaceutical industries.

KEYWORDS

Oleuropein; thermal decomposition behavior; kinetics process; thermogravimetry analysis

Nomenclature

dx/dt	A rate of conversion;
x	Conversion of the reaction, which is defined as $x = (w_0 - w_t)/(w_0 - w_f)$, where w_0 and w_f stand for the initial and final masses of the sample at each stage of decomposition (mg), respectively, and w_t stands for the mass of the sample at time t (mg);
$f(x)$	Differential mathematical model function of kinetics, which depends on the reaction type and behavior;
$g(x)$	Integral mathematical model function of kinetics, which depends on the reaction type and behavior;
$k(T)$	Temperature-dependent rate constant, which can be described by the Arrhenius equation;
A	Preexponential factor (min^{-1});

R Gas constant 8.314 J mol^{-1} K^{-1};
E Apparent activation energy (kJ mol^{-1});
T Absolute temperature (K);
B Heating rate (K min^{-1});
T_p Absolute thermodynamic temperature at which the mass loss rate reaches to a maximum value (K).

1 Introduction

As a cooking oil, the widespread use of olive oil has relations with low rates of cardiovascular disease in Mediterranean countries. Due to its high levels of polyphenols, olive oil has presented cardiovascular disease-preventing function. Oleuropein and hydroxytyrosol are the most representative polyphenols. Oleuropein, which is a natural secoiridoid glycoside [1], is the primary active compound of olive resources [2] and the chemical structural formula is presented in Fig. 1. Owing to hydroxyl active functional groups in chemical structure, oleuropein exhibits a variety of pharmacological activities. Based on the angle of the structure–activity relationship, its main pharmacological activities are closely related to its hydroxyl and aglycone structures. Extensive research efforts in the fields of medicine, food industry, and cosmetics have recently unveiled new pharmacological activities and mechanisms of action of oleuropein, mainly including antitumor [3,4], antioxidation [5], antimicrobial [6], antibacterial [7,8], hypoglycemic [9], and antihypertension activities, and coronary heart disease and atherosclerosis prevention function [10], among other biological activities. Used in cosmetics, food supplements and pharmaceuticals, olive leaf extract contains 15% to 30% oleuropein generally.

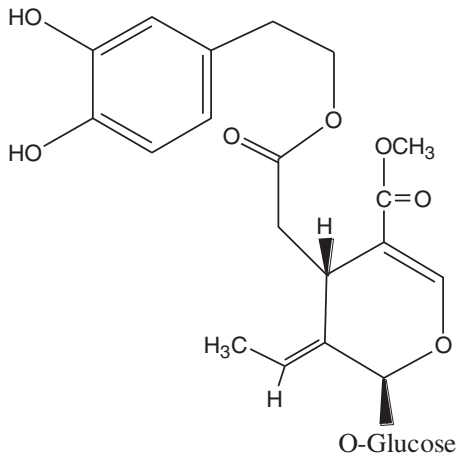

Figure 1: The chemical structural formula of oleuropein

Temperature and other processing conditions of olive leaves, such as drying treatment, extraction process, and storage after extraction, are known to affect the oleuropein stability on account of its multiple hydroxyl groups. Malik et al. [11] found that the original oleuropein level was preserved during the natural drying process of fresh olive leaves at 25°C, whereas drying at 60°C reduced. The active component of the oleuropein aqueous extract remained relatively stable for 7 days at room temperature; however, the degradation rate accelerated after 17 days. In addition, Xie et al. [12] discussed the effects of the temperature factor on oleuropein stability, finding that the degradation rate of oleuropein increased gradually with time. After 27 days, the degradation rate of oleuropein was 95.24% at 25°C and 38.1% at 4°C. This degradation was found to be related to the β-glucosidase contained in oleuropein.

Considering the important factors affecting the thermal stability of oleuropein for its related applications, gaining a deeper understanding of the specific degradation mechanisms is very significant. At present, the thermal analysis method has emerged as a promising technology to study drug thermal stability characteristics and kinetics decomposition behavior [13,14]. Furthermore, as determined by theoretical experimental studies, decomposition kinetics characteristic factors analysis has attracted much attention [15–18], mainly emphasizing on predicting material lifetimes and describing the thermodynamic properties in practical applications. The dynamic change of material weight with temperature can be determined using thermogravimetry (TG), and decomposition behavior and kinetics characteristic parameters are examined by different heating rates. Thus, the thermal decomposition stability and kinetics process of oleuropein could be investigated. According to a previously reported TG analysis [12], the decomposition of oleuropein began at 232.3°C. However, the specific thermal decomposition behavior and kinetics process remained unexplored.

In this current study, the oleuropein thermal stability was investigated by the thermal analysis method that involved weight change with temperature and the decomposition process. The effect of different heating rates on the oleuropein degradation kinetics behavior was examined, and the kinetics reaction behavior was simulated, and the relevant characteristic parameters were obtained to evaluate the degradation process. The current study would provide a systematic method for the analysis of the decomposition behavior and kinetics mechanism of oleuropein, and a theoretical basis to unveil its stability, quality control, and thermal processing as a drug.

2 Materials and Methods

2.1 Materials

Oleuropein (standard substance, purity > 98%, molecular weight 540) was purchased from Sigma Chemicals (St Louis, MO, USA).

2.2 Instrument and Methods

The thermogravimetric analyzer (NETZSCH TG 449C; Selb, Germany) was performed to investigate the oleuropein thermal stability, and the TG measurements were completed using about 10 mg sample in a nitrogen atmosphere of 313 to 1173 K (35 mL min^{-1}) at different heating rates (5, 10, 20, and 40 K min^{-1}). The kinetics decomposition behavior was studied by obtained data.

2.3 Kinetics Theoretical Analysis Methods of Thermal Decomposition

Eq. (1) is usually used to analyze the thermal decomposition kinetics theory.

$$\frac{dx}{dt} = k(T)f(x) \tag{1}$$

where $k(T)$ is rate constant, which is dependent only on the temperature, and it is usually calculated by the Arrhenius Eq. (2) as follows:

$$k(T) = Ae^{-E/RT} \tag{2}$$

where E is the activation energy and A is the Arrhenius preexponential factor.

When the heating rate (β) is dT/dt under non-isothermal condition, the mathematical expression of the thermal decomposition kinetics parameters can be expressed by Eq. (3) with substituting Eqs. (1) into (2) [19], and the corresponding kinetics parameters can be obtained on the basis of the TG result.

$$\frac{dx}{dt} = \beta \frac{dx}{dT} = Ae^{-E/RT} f(x) \; or \; \frac{dx}{dT} = \frac{A}{\beta} e^{-E/RT} f(x) \tag{3}$$

By integrating the above equation, it is expressed by Eq. (4):

$$g(x) = \frac{A}{\beta} \int_0^T e^{-E/RT} dT \tag{4}$$

and when

$$g(x) = \int_0^x \frac{1}{f(x)} dx \tag{5}$$

2.3.1 Kissinger Method

The mathematical theoretical expression of Kissinger method [20] is described as follows by Eq. (6):

$$\ln\left(\frac{T_P^2}{\beta}\right) = \ln\left(\frac{E}{R}\right) - \ln A + \frac{E}{RT_P} \tag{6}$$

By fitting $(T_p{}^2/\beta)$ against $1/T_p$, two constants of the slope *(E/R)* and intercept ln *(E/AR)* of the line can be obtained. Then, E and A can be calculated according to the binary first-order equation.

2.3.2 Flynn-Wall-Ozawa Method

The mathematical theoretical expression of the Flynn-Wall-Ozawa (F-W-O) method is expressed as follows by Eq. (7) [21]:

$$\ln \beta = \ln\left(\frac{AE}{R}\right) - \ln g(x) + 5.3305 - 1.052 \frac{E}{RT} \tag{7}$$

When the conversion rate (x) value is fixed, the value of ln ($AE/R\, g(x)$) can be regarded as a constant, and there is a linear relationship between ln β and $1/T$. Thus, with a given conversion rate, E can be calculated by the slope ($-1.052\ E/R$) of the line between ln β and $1/T$.

2.3.3 Friedman Method

The mathematical theoretical expression of the Friedman method [22] is represented as follows by Eq. (8):

$$\ln\left(\frac{dx}{dt}\right) = \ln[Af(x)] - \frac{E}{RT} \tag{8}$$

By plotting ln(dx/dt) against $1/T$, the slope ($-E/R$) of line is obtained, and E can be calculated.

2.4 The Most Probable Kinetics Reaction Behavior Model

In the study for a thermal decomposition behavior, choosing the probable kinetics reaction behavior model is important to reduce the difference between the mathematical models of theoretical kinetics reaction behavior and the actual kinetics reaction behavior. In order to select the most possible mathematical model of oleuropein dynamic behavior, the specific method is to combine the above four methods. Firstly, the integral forms of the 15 theoretical dynamic kinetics behavior functions [23] are respectively substituted into Eq. (9) (seen in Table 1), and the Coats-Redfern function is used to calculate the corresponding E value. Then, the range of E values closest to those calculated by Kissinger, F-W-O and Friedman methods is selected, and the corresponding theoretical mathematical model and reaction behavior is considered as the most possible kinetics behavior analysis of oleuropein.

Table 1: Kinetics behavior functions of pyrolysis

Number	Model	Reaction behavior	$g(x)$	$f(x)$
1 (F1)	Chemical reaction	$n = 1$	$-\ln(1-x)$	$1-x$
2 (F2)		$n = 2$	$(1-x)^{-1}-1$	$(1-x)^2$
3 (F3)		$n = 3$	$[(1-x)^{-2}-1]/2$	$(1-x)^3$
4 (D1)	Diffusion	One-dimensional diffusion	x^2	$1/2x^{-1}$
5 (D2)		Two-dimensional diffusion	$(1-x)\ln(1-x)+x$	$[-\ln(1-x)]^{-1}$
6 (D3)		Three-dimensional diffusion (Jander equation)	$[1-(1-x)^{1/3}]^2$	$3/2(1-x)^{2/3}[1-(1-x)^{1/3}]^{-1}$
7 (D4)		Three-dimensional diffusion (Ginstling-Brounshtein equation)	$(1-2x/3)-(1-x)^{2/3}$	$3/2[(1-x)^{-1/3}-1]^{-1}$
8 (A2)	Random nucleation and growth	Two-dimensional	$[-\ln(1-x)]^{1/2}$	$2(1-x)[-\ln(1-x)]^{1/2}$
9 (A3)		Three-dimensional	$[-\ln(1-x)]^{1/3}$	$3(1-x)[-\ln(1-x)]^{2/3}$
10 (R1)	Interfacial reaction	One-dimensional	x	1
11 (R2)		Cylindrical symmetry	$[1-(1-x)^{1/2}]$	$2(1-x)^{1/2}$
12 (R3)		Spherical symmetry	$[1-(1-x)^{1/3}]$	$3(1-x)^{2/3}$
13 (P2)	Exponential nucleation	Power function, $n = 1/2$	$x^{1/2}$	$2x^{1/2}$
14 (P3)		Power function, $n = 1/3$	$x^{1/3}$	$3x^{2/3}$
15 (P4)		Power function, $n = 1/4$	$x^{1/4}$	$3x^{3/4}$

The mathematical theoretical expression of the Coats-Redfern method [24] is represented as follows by Eq. (9):

$$\ln\frac{g(x)}{T^2} = \ln\frac{AR}{\beta E} - \frac{E}{RT} \tag{9}$$

The integral expressions g(x) of different reaction models are respectively substituted into Eq. (9), and two constants of the slope ($-E/R$) and intercept (ln ($AR/\beta E$)) of the fitting line are obtained by fitting ln[$g(x)/T^2$] and $1/T$. Thus, according to the two equations, E and ln A of corresponding models are calculated.

2.5 Calculation of lnA

The A is largely related only to the reactant (oleuropein) properties, not to the temperature parameters. Therefore, the calculation of A value is very important to determine the kinetics characteristic of oleuropein. Since E and ln A exist compensation effect, ln A is calculated usually by Eq. (10):

$$\ln A = aE + b \tag{10}$$

Firstly, the slope (a) and intercept (b) of the fitting line are obtained by fitting E and ln A under different β according to the data of the most suitable kinetics degradation reaction model. Then, the average E is substituted into Eq. (10) to calculate ln A.

3 Results and Discussion

3.1 Thermal Stability of Oleuropein

The thermogravimetry and differential thermogravimetry (TG/DTG) results for the oleuropein thermal decomposition were presented at 5, 10, 20, and 40 K min^{-1} heating rates in Figs. 2 and 3. As shown in Figs. 2, 3 and Table 2, the thermal decomposition process of oleuropein was comprised of two stages based on the data of 10 K min^{-1} heating rate. From Fig. 2 we can see that oleuropein was stable with little mass loss below 230.7°C, however, it started to decompose severely above this temperature. This result agreed with that reported by Xie et al. [12]. At approximately 339.2°C, the first stage of oleuropein decomposition was almost finished with 59.18% of residue. The second stage occurred from 339.2°C to 504.7°C, with 21.22% of residue. From Fig. 3 we can conclude that the first peak of the DTG curve appeared at 254.2°C with −4.36% min^{-1} maximum loss ratio. Furthermore, the second peak of the DTG curve and the maximum loss were 368.5°C and −3.27% min^{-1}, respectively.

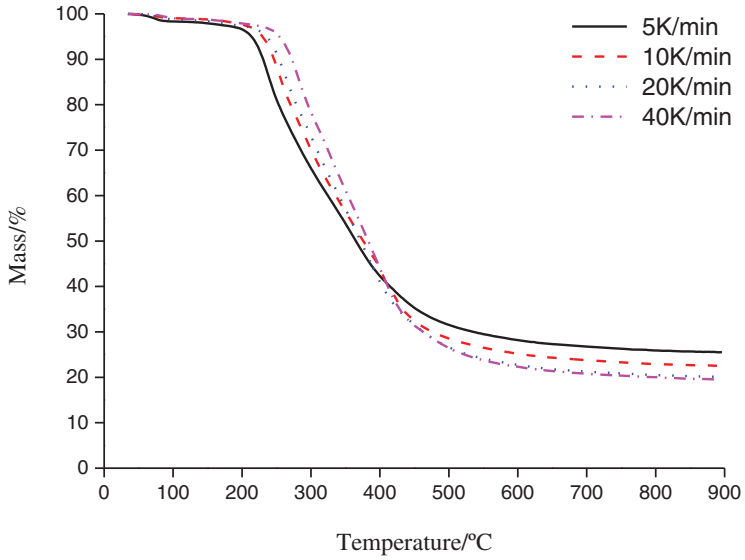

Figure 2: TG curve of oleuropein at different heating rates

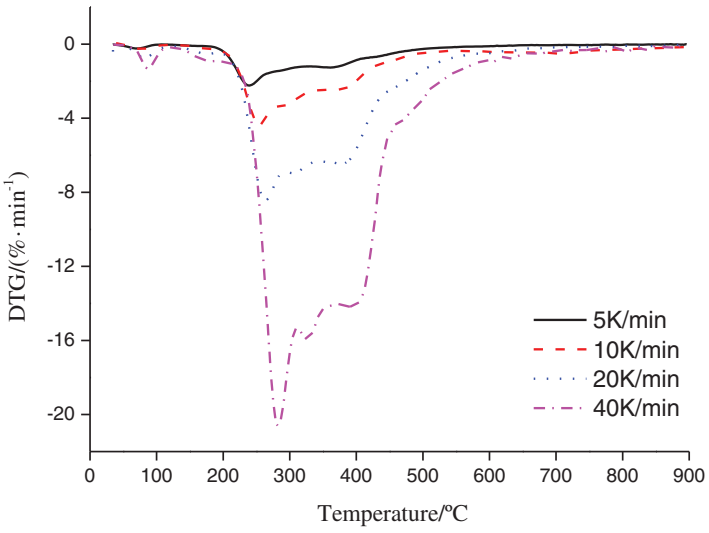

Figure 3: DTG curve of oleuropein at different heating rates

Table 2: The oleuropein thermal decomposition characteristic factors

Pyrolysis	Heating rate β(K·min^{-1})	Beginning temperature (°C)	End temperature (°C)	T_m (°C)	Max. loss ratio (%·min^{-1})	Residue (%)
First stage	5	215.4	331.2	239.2	−2.23	58.39
	10	230.7	339.2	254.2	−4.36	59.18
	20	238.7	345.4	263.4	−8.44	58.52
	40	257.3	374.3	282.6	−20.61	53.03
Second stage	5	331.2	491.3	360.6	−1.27	25.50
	10	339.2	504.7	368.5	−3.27	21.22
	20	345.4	509.1	379.2	−6.47	20.11
	40	374.3	517.3	398.0	−14.08	19.54

Note: T_m means the temperature with the maximum loss ratio.

Furthermore, the TG and DTG curves were presented basically at the same tendency with different heating rates of the oleuropein thermal decomposition. With the increase of heating rate, the thermal hysteresis phenomenon became more and more obvious, and the beginning and end decomposition temperature also increased, and the temperature peak corresponding to the maximum weight loss rate also shifted to a higher temperature region. This tendency was reported to agree with previous research [25]. Especially in the DTG curve, the temperature with the maximum loss ratio moved obviously to the right, which meant that the pyrolysis temperature required would be higher under the condition of the same weight loss rate. From a kinetics point of view, the thermal decomposition behavior had no connection with the heating rate, and it just depended on the temperature [26]. Too high heating rates would lead to an incomplete spectrum of part intermediate products, which had not enough time to separate each other. The effects of heating rates on thermal decomposition were mainly as follows: (1) With the heating rate increased, the time to obtain pyrolysis temperature was shortened, but the stopping time of volatiles was insufficient. In order to achieve full thermal decomposition, a higher temperature was needed. (2) Too high a heating rate would lead to the increase of temperature ladder inside and outside the raw material particles, and reduce the heat transfer efficiency of the thermal decomposition process. However, the heating rate was too low, which would lead to spectral discontinuity of the separated products and even serious trailing phenomenon. By fitting the data of T_m and β [27], the equations were obtained as follows: $T_m = 1.1426\beta + 511.58$ ($R^2 = 0.9493$) for the first stage and $T_m = 1.0419\beta + 630.19$ ($R^2 = 0.9923$) for the second stage, which showed that T_m were both closely related to β with a good positive correlation.

3.2 Non-Isothermal Kinetics Analysis of Oleuropein

The oleuropein non-isothermal thermal decomposition kinetics was calculated by the Kissinger, Friedman, F-W-O, and Coats–Redfern four theoretical analysis methods.

3.2.1 Kissinger Method

The kinetic factors of oleuropein thermal decomposition, calculated by Kissinger method, were presented in Table 3. According to Eq. (6), E and ln A of the first stage pyrolysis were 107.14 kJ mol^{-1} and 23.76 min^{-1}, respectively, and the linear correlation coefficient (R^2) was 0.9835. Furthermore, those of the second stage pyrolysis were 181.67 kJ mol^{-1} and 33.33 min^{-1}, with R^2 value of 0.9625. According to the obtained E values, the first stage of oleuropein decomposition was more favored than the second stage.

Table 3: Thermal decomposition kinetics factors of oleuropein by Kissinger method

Pyrolysis	E/(kJ·mol^{-1})	ln A	R^2
First stage	107.14	23.76	0.9835
Second stage	181.67	33.33	0.9625

3.2.2 Flynn-Wall-Ozawa Method and Friedman Method

Based on the Friedman and F-W-O methods, Es were obtained by Eqs. (6) and (7), and the corresponding kinetics decomposition data were presented in Tables 4 and 5. It was found that good R^2 values were obtained in all cases, and the E value increased with the conversion ratio from the kinetics data, which suggested that oleuropein decomposition was more difficult. As the conversion rate increased, the reaction activities of the products were more sensitive to temperature. The initial activation energy was lower, mainly because there were a large number of weak bonds (hydroxyl, hydrocarbon chain or carboxyl groups) in oleuropein during the initial pyrolysis, which were prone to fracture. With the increase in conversion rate, it was mainly the thermal decomposition of the benzene ring or glycosidic bond, in which the fracture of strong bonds needed more energy consumption, manifested by higher activation energy. Therefore, the E mean values were needed to calculate, and were 168.98 and 142.30 kJ mol^{-1} in the first stage and 299.06 and 236.38 kJ mol^{-1} in the second stage using Friedman and F-W-O methods, respectively.

Table 4: Kinetics data of oleuropein thermal decomposition by Friedman and F-W-O methods

Pyrolysis	Conversion x	β							
		5 °C/min		10 °C/min		20 °C/min		40 °C/min	
		dx/dt	t	dx/dt	t	dx/dt	t	dx/dt	t
First stage	0.1	−2.030	230.43	−4.036	246.72	−7.667	253.77	−17.943	272.05
	0.15	−2.222	241.11	−4.328	256.72	−8.405	265.98	−20.579	283.75
	0.2	−1.892	253.33	−3.642	269.22	−7.414	279.21	−17.925	295.46
	0.25	−1.565	268.09	−3.371	284.22	−6.865	293.97	−15.328	310.21
	0.3	−1.435	285.39	−3.214	299.22	−6.603	308.73	−14.795	324.46
	0.35	−1.290	303.71	−2.787	316.72	−6.458	324.50	−14.422	338.71
	0.4	−1.207	324.06	−2.547	334.22	−6.330	340.28	−14.206	353.47
Second stage	0.1	−1.255	355.62	−2.465	364.22	−6.400	364.20	−14.181	389.60
	0.15	−1.247	366.81	−2.442	376.72	−6.450	372.85	−14.091	397.24
	0.2	−1.153	378.52	−2.337	386.72	−6.443	382.01	−13.900	404.87

Table 5: Kinetics factors of oleuropein thermal decomposition by Friedman and F-W-O methods

Pyrolysis	Conversion (x)	Friedman method		F-W-O method	
		E/kJ mol^{-1}	R^2	E/kJ mol^{-1}	R^2
First stage	0.1	122.01	0.9842	111.33	0.9766
	0.15	126.44	0.9907	113.02	0.9884

(Continued)

Table 5 (continued)

Pyrolysis	Conversion (x)	Friedman method		F-W-O method	
		E/kJ mol^{-1}	R^2	E/kJ mol^{-1}	R^2
	0.2	134.97	0.987	119.26	
	0.25	144.70	0.9931	125.89	0.9906
	0.3	174.12	0.9951	143.27	0.9931
	0.35	211.98	0.9862	169.62	0.9895
	0.4	268.65	0.9763	213.70	0.9832
	mean	168.98	—	142.30	—
Second stage	0.1	251.14	0.9851	200.67	0.9847
	0.15	289.95	0.9954	231.72	0.9999
	0.2	356.08	0.9932	276.74	0.9988
	mean	299.06	—	236.38	—

Note: "—" means without this value.

The average E values for the first and second stages obtained by the Friedman method were a litter higher than those obtained by the F-W-O method in Table 5. Furthermore, combined Table 3, it was shown that the Kissinger method was the lowest value among the three methods. The significant difference was due to the fact that the equation of the Kissinger method assumed that the kinetic factors of temperature and E were independent of the conversion degree [28,29]. In conclusion, it could be concluded that the E calculation results of these three methods, with oleuropein thermal decomposition in the first and second stages, were in the range of 107.14–168.98 and 181.67–299.06 kJ mol^{-1}, respectively.

3.2.3 Coats-Redfern Method

In Table S1, the main kinetics factors of oleuropein thermal decomposition by the Coats–Redfern method were presented with the heating rates (5–40 K min^{-1}), and it was concluded that E values increased with 5–40 K min^{-1}, because more energy was required to decompose oleuropein at higher heating rates. Moreover, except for the P3 and P4 models, the fitting results of 13 models had good linear correlation, and E and ln A all showed clear differences. Therefore, a good linear dependence was not sufficient to select the most appropriate reaction model. The current study combined the Kissinger method, Friedman method, F-W-O method, and Coats-Redfern method, the four methods were used to screen and verify the E value and the most suitable kinetics degradation reaction model for the thermal decomposition process of oleuropein [30].

3.2.4 Calculation of ln A

The E values, obtained using the above-mentioned three methods for the first stage, ranged between 107.14 and 168.98 kJ mol^{-1}. Considering the linear dependence of the fitting results, D3 was the best model, which afforded E values of 131.73–151.86 kJ mol^{-1}. In consequence, the diffusion model and three-dimensional diffusion Jander equation reaction behavior (D3) could describe exactly the first stage of oleuropein thermal decomposition. The integral function for the reaction model was $g(x) = \left[1 - (1-x)^{\frac{1}{3}}\right]^2$, and the differential function was $f(x) = \frac{3}{2}(1-x)^{\frac{2}{3}}\left[1 - (1-x)^{\frac{1}{3}}\right]^{-1}$.

As shown in Fig. 4, $\ln A = 0.20E - 2.4$ was obtained by fitting the data calculated from the D3 model, and it was used to resolve the kinetics compensation effect for the first stage of oleuropein pyrolysis. Firstly, corresponding E_0 was calculated as the mean of E with different heating rates in model D3, and was obtained for 143.72 kJ mol^{-1}. Secondly, ln A was 26.34 min^{-1} through E_0 based on the above-mentioned compensation effect fitting the linear equation. Finally, The differential form $f(x) = \frac{3}{2}(1-x)^{\frac{2}{3}}\left[1-(1-x)^{\frac{1}{3}}\right]^{-1}$, E_0, and A were substituted into Eq. (3), resulting in the following kinetics expression for the first stage of oleuropein thermal decomposition: $\frac{dx}{dT} = \frac{2.75\times10^{11}}{\beta}\exp\left(-\frac{1.44\times10^{5}}{8.314\times T}\right) \times \frac{3}{2}(1-x)^{\frac{2}{3}}\left[1-(1-x)^{\frac{1}{3}}\right]^{-1}$.

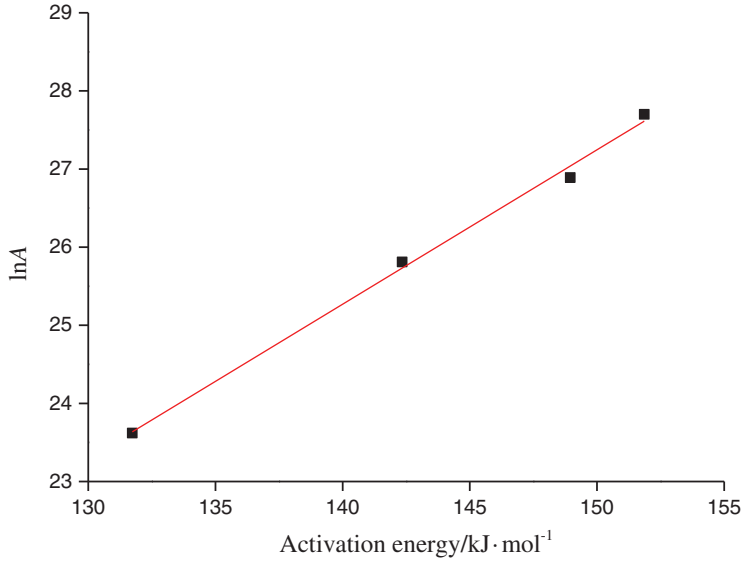

Figure 4: Kinetics compensation effect of the first stage of oleuropein pyrolysis by different heating rates

In the second stage of oleuropein pyrolysis, the kinetics characteristic factors, which were summarized in Table S1, were calculated by the Coats–Redfern method. The above-mentioned three methods afforded a range of E values for the second stage of 181.67–299.06 kJ mol^{-1}, and model D1 was the closest with the range of E (195.53–328.24 kJ mol^{-1}). Therefore, the one-dimensional diffusion reaction behavior (D1 model) could describe exactly the second stage of the oleuropein thermal decomposition process. The integral function for the reaction model was $g(x) = x^2$, and the differential function was $f(x) = 1/2x^{-1}$.

By fitting the data of E and ln A calculated from the D1 model, $\ln A = 0.19E - 4.48$ was obtained. For the second stage of oleuropein pyrolysis, the kinetics compensation effect at different heating rates was presented in Fig. 5. Then, according to the E calculated by model D1 at different heating rates, the mean E_0 value was 247.01 kJ mol^{-1}, and ln A was calculated to 42.45 min^{-1} by the above-mentioned fitting linear equation. Finally, the kinetics function was obtained by substituting $f(x) = 1/(2x)$, E_0, and A into Eq. (3), and the final equation for the second stage of oleuropein thermal decomposition was expressed as follows: $\frac{dx}{dT} = \frac{2.23\times10^{18}}{\beta}\exp\left(-\frac{2.47\times10^{5}}{8.314\times T}\right) \times \frac{1}{2x}$.

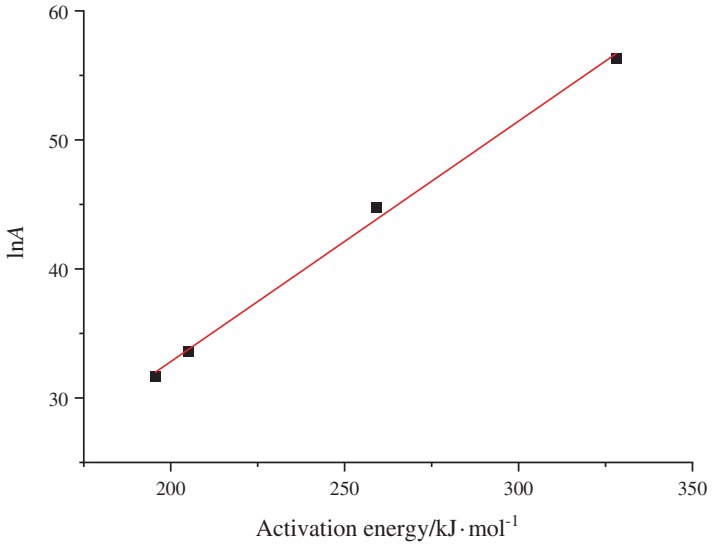

Figure 5: Kinetics compensation effect of the second stage of oleuropein pyrolysis by different heating rates

3.2.5 Proposed Mechanism of Oleuropein Thermal Decomposition

From the TG/DTG results for the oleuropein thermal decomposition (the rate was 10 K/min), we could see that oleuropein was degraded from 230.7°C to 339.2°C firstly, with 59.18% of residue. The second stage occurred at 339.2°C, and was almost finished with 21.22% of residue at approximately 504.7°C. Due to multiple hydroxy groups, it produced water at the beginning. According to the oleuropein acidic and enzymatic hydrolysis processes and products, the main chemical bond ruptures existed at the ester bond and glycosidic bond in the chemical structure, presented in Fig. 6.

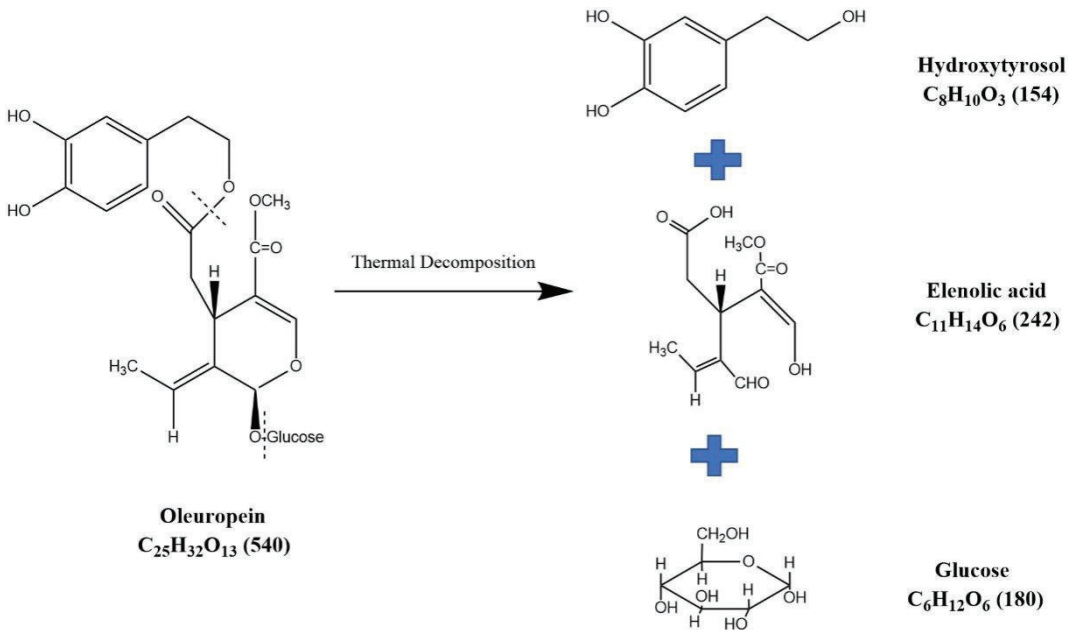

Figure 6: Oleuropein thermal decomposition

From the reference [25], we could conclude that the main decomposition process of hydroxytyrosol started at 262.8°C, and ended at 409.7°C. A solid residue of 2.68% was observed, and the final products were CO_2, water, and 2.68% solid char. According to the TG diagram of hydroxytyrosol pyrolysis, the residual weight was about 13% at 339.2°C. As reported in reference [31], the glucose was decomposed from 190°C, and the weight loss rate gradually decreased from about 379°C until the end of the pyrolysis process. At the end of the 600°C pyrolysis reaction, the total weight loss of the sample was 85% of the initial weight. The primary products of glucose pyrolysis were water, furfural, CO_2 and other products. According to the TG diagram of glucose pyrolysis, the residual weight was about 34% at 339.2°C. Therefore, at the end temperature of the first stage of oleuropein decomposition (339.2°C), the weights of volatile substances were calculated by hydroxytyrosol molecular weight multiply (1%–13%) and glucose molecular weight multiply (1%–34%), and the result (253) was close to oleuropein experimental value (221). Moreover, at the end temperature of the second stage of oleuropein decomposition (504.7°C), the hydroxytyrosol had 2.68% residue and glucose had 18% residue. In the experimental result, the second stage of oleuropein was with 21.22% of residue, and it could be inferred that elenolic acid was nearly decomposed completely in this stage. So, oleuropein was firstly decomposed for hydroxytyrosol, elenolic acid and glucose, and these substances were further degraded. In summary, the pyrolysis products of oleuropein mainly consisted of solid char, water, CO_2 and furfural, according to pyrolysis products of hydroxytyrosol and glucose.

4 Conclusion

The thermal decomposition stability and kinetics behavior of oleuropein from olive plants were studied by TG analysis and non-isothermal theoretical method. The TG-DTG results revealed that oleuropein decomposition consisted of two stages, the first of which started at 230.7°C and the second at 339.2°C. The oleuropein decomposition process of the first stage followed a non-isothermal kinetics behavior described with a D3 model (three-dimensional diffusion, Jander equation), and the second stage with a D1 model (one-dimensional diffusion). In addition, by combining the abovementioned four methods, E and ln A were both calculated. It was inferred that the pyrolysis products of oleuropein mainly consisted of solid char, water, CO_2 and furfural. Therefore, this present research would provide new theoretical information on the thermal decomposition behavior of oleuropein, and suggests its suitability for low-temperature applications in cosmetic, food supplement and pharmaceutical industries.

Funding Statement: This work was funded by Guangdong Basic and Applied Basic Research Foundation (No. 2019A1515111159), Characteristic Innovative Projects for Education Department of Guangdong Province 2021 Year (No. 2021KTSCX302).

Conflicts of Interest: The authors declared that they had no conflicts of interest to report regarding the present study.

References

1. Zhang, Y. G., Zhang, X. J., Xin, E. D. et al. (2019). Research statue on pharmacological action of Oleuropein. *The Chinese Journal of Clinical Pharmacology, 35(24),* 3265–3268.
2. Wang, H., Li, M. S., Zhu, L. Y., Zhou, L. P. (2018). Research progress on the oleuropein-a natural antioxidants from *Oleaceae*. *Northern Horticulture, 42(5),* 170–177.
3. Kimura, Y., Wu, N. (2019). Olive leaf extract and its main component oleuropein prevent chronic ultraviolet B radiation-induced skin damage and carcinogenesis in hairless mice. *Journal of Nutrition, 139(11),* 2079–2086.
4. Sherif, I. O., Al-Gayyar, M. M. H. (2018). Oleuropein potentiates anti-tumor activity of cisplatin against HepG2 through affecting proNGF/NGF balance. *Life Sciences, 198,* 87–93.

5. Wang, B., Shen, S., Qu, J., Xu, Z., Feng, S. et al. (2021). Optimizing total phenolic and oleuropein of Chinese olive (*Olea europaea*) leaves for enhancement of the phenols content and antioxidant activity. *Agronomy, 11(4),* 686. https://doi.org/10.3390/agronomy11040686
6. Topuz, S., Bayram, M. (2021). Oleuropein extraction from leaves of three olive varieties (*Olea europaea* L.): Antioxidant and antimicrobial properties of purified oleuropein and oleuropein extracts. *Journal of Food Processing and Preservation, 46(6),* e15697.
7. Yuan, J. J., Tu, J. L., Qin, F. G., Xu, Y. J., Li, B. (2018). Phenolic composition of oleuropein extract after enzymatic process by HPLC-MS and their antioxidant and antibacterial activities. *Journal of Food Biochemistry, 42(3),* e12517. https://doi.org/10.1111/jfbc.12517
8. Munekata, P. E., Nieto, G., Pateiro, M., Lorenzo, J. M. (2020). Phenolic compounds obtained from *Olea europaea* by-products and their use to improve the quality and shelf life of meat and meat products–A review. *Antioxidants, 9(11),* 1061. https://doi.org/10.3390/antiox9111061
9. Mohamed, N. A., Abdou, H. M., Marzouk, M. M. (2018). Antidiabetic and immunomodulatory effects of oleuropein and vitamin C in diabetic male rats. *Journal of Advances in Biology, 11,* 2250–2268.
10. Menezes, R. C. R., Peres, K. K., Costa-Valle, M. T., Faccioli, L. S., Dallegrave, E. et al. (2022). Oral administration of oleuropein and olive leaf extract has cardioprotective effects in rodents: A systematic review. *Revista Portuguesa de Cardiologia, 41(2),* 167–175.
11. Malik, N. S. A., Bradford, J. M. (2008). Recovery and stability of oleuropein and other phenolic compounds during extraction and processing of olive (*Olea europaea* L.) leaves. *Journal of Food Agriculture and Environment, 6(2),* 1–8.
12. Xie, P. J., Huang, L. X., Zhang, C. H. (2013). Stability of oleuropein in olive leaves extracts and its chelating action to ferrous ions. *Science and Technology of Food Industry, 4,* 133–136.
13. Ma, Y. Y., Chen, J. H., Wang, H. X., Chen, Q., Zhang, M. (2019). Stability and degradation kinetics of anthocyanins from *Dendrobium officinale*. *Science and Technology of Food Industry, 40(16),* 50–57.
14. Campostrini, R., Grigiante, M., Brighenti, M. (2021). Potentialities of mass spectrometry on activation energy and secondary reactions determination of calcium oxalate thermal decomposition. *International Journal of Chemical Kinetics, 53(10),* 1082–1100.
15. Pan, Y., Liang, Y., Ma, R., Ruan, L., Wang, S. L. (2021). Stability and degradation kinetics of anthocyanins from red cabbage. *Science and Technology of Food Industry, 42(5),* 51–59.
16. Bao, Y. H., Cao, W. H., Fu, Q., Zhang, H. T., Lu, W. H. et al. (2020). Antimicrobial activity and thermal degradation kinetics of total alkaloids from *Berberis poireti*. *Modern Food Science and Technology, 36(3),* 39.
17. Barbosa, H. F., Francisco, D. S., Ferreira, A. P., Cavalheiro, É. T. (2019). A new look towards the thermal decomposition of chitins and chitosans with different degrees of deacetylation by coupled TG-FTIR. *Carbohydrate Polymers, 225,* 115232.
18. Wang, Z. H., Wang, C. Z., Peng, M. (2019). Thermal decomposition kinetics of raw and treated olive waste. *Thermal Science, 23(6A),* 3501–3512.
19. Lu, C. W., Xi, T. G. (2002). *Thermal analysis mass spectrometry.* Shanghai, China: Shanghai Science and Technology Literature Press.
20. Rotaru, A., Moanță, A., Rotaru, P., Segal, E. (2009). Thermal decomposition kinetics of some aromatic azomonoethers. *Journal of Thermal Analysis and Calorimetry, 92,* 233–238.
21. Venkatesh, M., Ravi, P., Tewari, S. P. (2013). Isoconversional kinetic analysis of decomposition of nitroimidazoles: Friedman method *vs*. Flynn-Wall-Ozawa method. *Journal of Physical Chemistry A, 117(40),* 10162–10169.
22. Corradini, E., Teixeira, E. M., Paladin, P. D., Agnelli, J. A., Silva, O. R. R. F. et al. (2009). Thermal stability and degradation kinetic study of white and colored cotton fibers by thermogravimetric analysis. *Journal of Thermal Analysis and Calorimetry, 97(2),* 415–419. https://doi.org/10.1007/s10973-008-9693-8
23. Hao, Y. R. (2012). *Study on pyrolysis kinetic of biomass residue (Master Thesis)*. Nanjing University of Science and Technology, Nanjing, China.

24. Naqvi, S. R., Uemura, Y., Osman, N., Yusup, S. (2015). Kinetic study of the catalytic pyrolysis of paddy husk by use of thermogravimetric data and the Coats-Redfern model. *Research on Chemical Intermediates, 41(12),* 1–13. https://doi.org/10.1007/s11164-015-1962-0
25. Tu, J. L., Yuan, J. J. (2018). Thermal decompositionbehavior of hydroxytyrosol (HT) in nitrogen atmosphere based on TG-FTIR methods. *Molecules, 23(2),* 404. https://doi.org/10.3390/molecules23020404
26. Lopez-Velazquez, M. A., Santes, V., Balmaseda, J., Torres-Garcia, E. (2013). Pyrolysis of orange waste: A thermo-kinetic study. *Journal of Analytical and Applied Pyrolysis, 99(1),* 170–177. https://doi.org/10.1016/j.jaap.2012.09.016
27. Liu, J. L. (2011). *Study on directed pyrolysis of lignocellulosic biomass (Doctor Thesis)*. Chinese Academy of Forestry, Beijing, China.
28. Salehi, M., Clemens, F., Graule, T., Grobéty, B. (2012). Kinetic analysis of the polymer burnout in ceramic thermoplastic processing of the YSZ thin electrolyte structures using model free method. *Applied Energy, 95(2),* 147–155. https://doi.org/10.1016/j.apenergy.2012.02.025
29. Aburto, J., Moran, M., Galano, A., Torres-García, E. (2015). Non-isothermal pyrolysis of pectin: A thermochemical and kinetic approach. *Journal of Analytical and Applied Pyrolysis, 112(3),* 94–104. https://doi.org/10.1016/j.jaap.2015.02.012
30. Yuan, J. J., Tu, J. L., Xu, Y. J., Qin, F. G., Li, B. et al. (2018). Thermal stability and products chemical analysis of olive leaf extract after enzymolysis based on TG-FTIR and Py-GC–MS. *Journal of Thermal Analysis & Calorimetry, 132(3),* 1729–1740. https://doi.org/10.1007/s10973-018-7083-4
31. Deng, C. (2015). *Experimental study on Pyrolysis of glucose and its derivatives based on TGA-GC-MS (Master Thesis)*. Huazhong University of Science and Technology, China.

Supplementary Materials

Table S1: Kinetics parameter of oleuropein thermal decomposition by coats-redfern method

Pyrolysis	No.	β = 5 K min^{-1}			β = 10 K min^{-1}			β = 20 K min^{-1}			β = 40 K min^{-1}		
		E /kJ mol^{-1}	ln A	R^2	E /kJ mol^{-1}	ln A	R^2	E /kJ mol^{-1}	ln A	R^2	E /kJ mol^{-1}	ln A	R^2
First stage	F1	63.45	11.04	0.9828	68.78	12.51	0.9746	70.34	13.39	0.9871	73.44	14.14	0.9923
	F2	69.28	12.57	0.9854	75.07	14.11	0.9779	78.10	14.84	0.9893	80.10	15.75	0.9939
	F3	75.41	14.17	0.9876	81.70	15.78	0.9806	84.16	16.36	0.9912	87.11	17.43	0.9953
	D1	124.44	23.95	0.9825	134.48	26.06	0.9747	140.76	26.52	0.9867	143.52	27.94	0.9916
	D2	128.02	24.17	0.9833	138.34	26.32	0.9757	140.29	27.70	0.9874	147.62	28.21	0.9922
	D3	131.73	23.62	0.9842	142.34	25.81	0.9767	148.95	26.89	0.9882	151.86	27.70	0.9927
	D4	129.25	22.99	0.9836	139.38	25.15	0.9760	144.50	26.49	0.9877	149.03	27.04	0.9924
	A2	27.45	2.71	0.9768	29.97	3.81	0.9666	30.69	4.51	0.9822	32.09	5.31	0.9898
	A3	15.44	−0.36	0.9674	17.04	0.62	0.9542	17.80	0.98	0.9740	18.31	2.08	0.9858
	R1	57.94	9.58	0.9797	62.82	10.99	0.9709	65.89	10.99	0.9844	67.14	12.61	0.9903
	R2	60.66	9.61	0.9813	65.76	11.05	0.9729	67.58	11.05	0.9858	70.24	12.67	0.9914
	R3	61.58	9.44	0.9818	66.76	10.90	0.9735	68.49	11.52	0.9862	71.30	12.52	0.9917
	P2	24.69	1.92	0.9720	26.99	2.99	0.9607	27.96	3.68	0.9778	28.94	4.48	0.9868
	P3	13.61	−0.94	0.9590	15.05	0.02	0.9442	15.98	0.82	0.9662	16.21	1.48	0.9811
	P4	8.06	−2.60	0.9351	9.08	−1.67	0.9156	9.50	−1.09	0.9434	9.84	−0.24	0.9710
Second stage	F1	100.97	15.21	0.9896	105.98	16.59	0.9997	135.41	23.10	0.9888	172.56	29.72	0.9923
	F2	109.96	17.07	0.9915	115.32	18.49	0.9999	147.21	25.47	0.9907	187.36	32.54	0.9938
	F3	119.45	19.02	0.9930	125.14	20.48	0.9999	159.63	27.95	0.9923	202.94	35.50	0.9951
	D1	195.53	31.63	0.9887	205.05	33.60	0.9994	259.23	44.79	0.9877	328.24	56.28	0.9912
	D2	201.05	32.05	0.9894	210.78	34.05	0.9995	266.47	45.52	0.9884	337.32	57.57	0.9917
	D3	206.79	31.71	0.99	216.73	33.73	0.9996	273.98	45.50	0.9891	346.74	57.57	0.9923
	D4	202.97	30.93	0.9896	212.76	32.94	0.9995	268.97	44.51	0.9886	340.47	56.39	0.9919
	A2	45.16	4.85	0.9869	47.60	5.90	0.9996	62.33	9.65	0.9868	80.71	13.41	0.9912
	A3	26.56	1.13	0.9830	28.14	2.08	0.9995	37.97	4.93	0.9841	50.09	7.75	0.9898
	R1	92.44	13.44	0.9874	97.13	14.79	0.9993	124.24	20.86	0.9866	158.55	27.04	0.9905
	R2	96.64	13.62	0.9885	101.50	14.98	0.9995	129.75	21.27	0.9878	165.46	27.67	0.9915
	R3	98.07	13.51	0.9889	102.98	14.88	0.9996	131.62	21.24	0.9881	167.80	27.71	0.9917
	P2	40.90	3.91	0.9837	43.18	4.94	0.9990	56.75	8.48	0.9839	73.70	12.02	0.9890
	P3	23.72	0.45	0.9784	25.19	1.39	0.9987	34.25	4.11	0.9804	45.42	6.78	0.9871
	P4	15.13	−1.45	0.9701	16.20	−0.55	0.9981	23.01	1.78	0.9755	31.28	4.03	0.9847